TUDelft

Delft University of Technology

FLEXOP – Application of aeroelastic tailoring to a flying demonstrator wing

Meddaikar, Yasser; Dillinger, Johannes; Sodja, Jurij; De Breuker, Roeland

FLEXOP – APPLICATION OF AEROELASTIC TAILORING TO A FLYING DEMONSTRATOR WING

M.Y. Meddaikar[1*], J. K. S. Dillinger[1], J. Sodja[2], R. de Breuker[2]

[1] DLR – Institute of Aeroelasticity, Göttingen, Germany
[2] Delft University of Technology - Aerospace Structures and Computational Mechanics, Delft, The Netherlands

Abstract
This paper presents the application of aeroelastic tailoring in the design of flying demonstrator wings. The work is part of the Flutter Free Flight Envelope eXpansion (FLEXOP) project, funded under the Horizon 2020 framework. The project involves the design, manufacturing and flight-testing of a UAV toward two principle goals: i) to demonstrate the passive load alleviation potential through composite tailoring, ii) to validate methods and tools for flutter modelling and flutter control. The work presented here addresses the first of the above mentioned goals.
The design of the primary load-carrying wing-box in this task is performed using a joint DLR – TU Delft optimization strategy. In total, two sets of wings are designed in order to demonstrate the potential benefits of aeroelastic tailoring – i) a reference wing wherein the laminates of the wing-box entities are restricted to balanced and symmetric laminates; ii) a tailored wing wherein the laminates are allowed to be unbalanced, hence enhancing the bending-torsion coupling essential for aeroelastic tailoring.
The optimized design is then manufactured and extensively tested to validate and improve the simulation models corresponding to the wing design. Flight tests are scheduled to be performed in late 2018 to demonstrate the load alleviation capabilities attained through the applied aeroelastic tailoring.

Keywords
Aeroelastic tailoring, UAV, Composite optimization, FLEXOP

1. INTRODUCTION

The Flutter-free Flight Envelope Extension for Economical Performance Improvement or FLEXOP [1], is a European research project aiming to develop and demonstrate technological concepts to improve performance of flexible, high-aspect ratio, swept aircraft wings. In particular, load alleviation techniques through aeroelastic tailoring and active flutter control are to be demonstrated on an unmanned flying aircraft [2]. The methods and concepts developed will then be applied to the design of a full-scale aircraft in a scale-up task.

The design and testing of a commercial-scale aircraft with new technologies is usually a cost-prohibitive exercise. Within the FLEXOP project, an unmanned aircraft vehicle (UAV) [2]–[4] is instead put through a complete aircraft design cycle, with the goal of applying the new technologies mentioned above.

The FLEXOP UAV will be designed, manufactured and tested, using three different wing-pairs. Two wing configurations target demonstrating aeroelastic tailoring [5] and are presented in this paper. A third wing [6] is designed to flutter within the test regime and will include a flutter-suppression control algorithm.

The use of composite materials in aircraft structures offers several advantages over conventional metals. Among others, the directional nature of composite stiffness can be optimized such that favorable aeroelastic effects are exploited. This interactive subject involving composite optimization considering or targeting aeroelastic effects is known as aeroelastic tailoring.

Aeroelastic tailoring has been studied extensively in the past for several applications [7]–[15]. Experimental studies in wind-tunnel experiments have also been presented in recent works [16]–[18]. Application of aeroelastic tailoring to an actual flying aircraft and a validation of an aeroelastic tailoring framework however is still missing and is hence the aim of this work.

The design cycle involved in the FLEXOP aeroelastically tailored wings is presented in this paper. Two pairs of wings are designed. The first pair of wings serves as the reference wing in the project and is designed using more conventional balanced-symmetric laminates. The second pair of wings also allows for unbalanced laminates, thus allowing a much larger design space and exploitation of composite coupling benefits.

Figure 1: Schematic of the FLEXOP UAV demonstrator

The wing structure is optimized using an aeroelastic tailoring toolchain, developed at the Delft University of Technology (TUD) and DLR-Institute of Aeroelasticity (DLR). The first step of this work-flow is presented in

detail in [5]. The wings are then manufactured based on the outcome of the optimization task. Static tests are performed to characterize the stiffness behavior of the actual manufactured wings. An airworthiness test is then performed, where the wing is subjected to the limit loads it was designed for, using sand-bags. In the upcoming months, a ground vibration test (GVT) will performed to obtain the dynamic response of the wings, using which the finite element (FE) models will be updated. Finally, flight tests are planned with the UAV and a large set of flight data will be recorded to validate the design process.

At the time of writing of this paper, the reference wings have been manufactured and are hence elaborated upon in the ground-testing sections.

2. AEROELASTIC TAILORING FRAMEWORK

The aeroelastic tailoring approach applied in this work is essentially a multi-fidelity approach. The design space for the design of aeroelastically tailored wings is very large due to the large number of design variables and constraints that are typically associated with this type of problem. The following sequential approach is hence implemented and is summarized in Figure 2.

1. A low-fidelity beam-model based stiffness-optimization tool PROTEUS. This step is used to perform initial design-studies to explore the vast design-space. The optimized design from this step serves as the initial design for the second step in the toolchain.

2. A high-fidelity shell-model based genetic algorithm (GA) for stacking sequence optimization. The outcome of this step is the layup plan that is required for manufacturing.
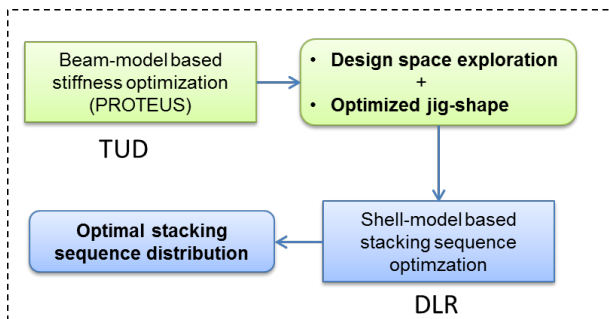

Figure 2: Two-step DLR–TUD aeroelastic tailoring workflow

The premise behind using this two-step approach is that using the low-fidelity design tool in the first step, an extensive design-study is performed wherein effects of different material types, laminate reference coordinate system definitions and wingbox layout is studied. Additionally, the optimized design obtained from this step serves as the starting point in the second optimization step for faster overall convergence. The second optimization step uses a shell-based NASTRAN FE model of a higher-fidelity, within a discrete GA for stacking sequence optimization.

2.1 Beam-model based stiffness-optimization

The first step in the optimization toolchain is performed using the design tool, PROTEUS, developed at TUD. The tool is an aeroelastic wing design tool developed to

improve the conceptual design of aircraft wings by considering aeroelastic effects. In this regard, the tool is computationally-efficient to enable quick design optimization studies.

A detailed explanation of the design tool is presented in [19]. The key aspects of the design tool are summarized as follows.

- A 3d cross-sectional modeler [20] compiles the wing cross-sectional properties into equivalent Timoshenko stiffness matrices.

- A static aeroelastic analysis combines a geometrically non-linear Timoshenko beam model [21] based on the co-rotational formulation, to the steady vortex lattice method (VLM) - based aerodynamic model [22].

- A linear dynamic aeroelastic analysis which linearizes the stiffness matrix around the non-linear static equilibrium solution. This is then coupled to a mass matrix and an aerodynamic model based on the unsteady VLM [22].

For the optimization a lamination parameter - based approach is used. The stiffness of the composite laminates is represented here by so-called lamination parameters. These parameters encapsulate the stiffness behavior of a composite laminate as convenient continuous design variables. The lamination parameters together with the laminate thickness are the design variables in this step. Lamination parameters [20], [21] present a very useful parametrization scheme for composite laminates and have been extensively applied in the past, with some of the early works presented in [23]–[25].

2.2 Shell-model based stacking sequence optimization

The design obtained in the previous step represents the optimal stiffness distribution in the structure. This design is used as a starting point in this second optimization step.

The key aspects of the stacking sequence optimization step are listed below.

- A genetic algorithm (GA) using a technique known as stacking sequence tables (SST) [26], [27]. The GA with SST follows rules of generalized laminate blending [28] to ensure ply continuity between adjacent design fields and also provides information on ply-drop sequence. The GA also includes several industry-standard design guidelines related to laminate and ply-drop requirements.

- An aeroelastic tailoring framework established in [12], [20]. The framework uses NASTRAN to generate the required optimization responses and sensitivities.

- A NASTRAN shell-element based modelling strategy coupled with a doublet lattice model (DLM) for the aerodynamics. The aeroelastic model is then obtained through splining between the structural and aerodynamic models. The generation of the structural, aerodynamic and optimization models is carried out using an in-house model generator

ModGen [29].

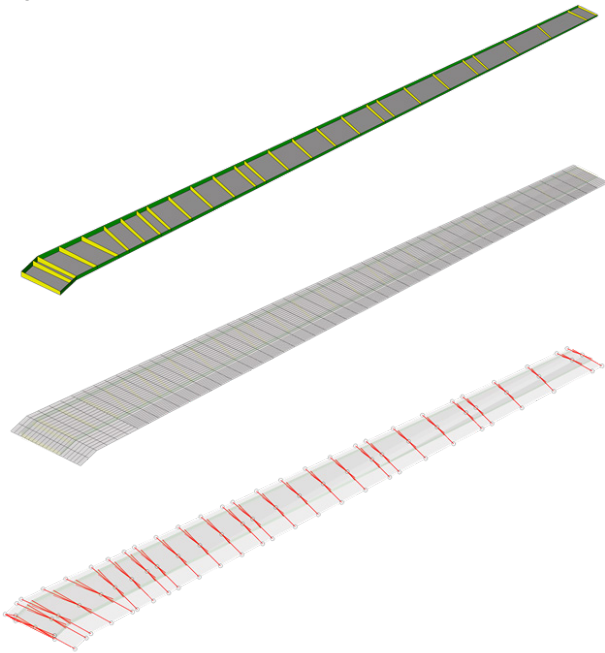A schematic of the FLEXOP wing models is shown in Figure 3.

Figure 3: NASTRAN models used in Step 2 of the optimization workflow – structural FE model, aerodynamic DLM model, coupled aeroelastic splining model

3. WING SPECIFICATIONS

3.1 Planform and design

The UAV wings follow a traditional wing-box concept – comprising of upper and lower skins, ribs and spars. The wings have a full span of ~7m, an aspect ratio of 16.33, a leading backward-sweep angle of 20° and a custom unsymmetric airfoil. Stringers are not used in the design given the dimensions of the wing. The key design specifications of the wing are listed in Table 1.

A carbon-fiber/epoxy material with the technical specification Hexcel 8552/34%/UD134/AS4Tape is used in the design.

Table 1: Design specifications of the wings

Planform properties	
span	3.536m
root chord	0.4713m
tip chord	0.2357m
leading edge sweep	20°
airfoil thickness - root	10% chord
airfoil thickness - tip	8% chord
Wing box	
front spar position	15% chord
rear spar position	71% chord
Operating requirements	
atmosphere	ISA

cruise speed	45m/s (TAS)
cruise altitude ASL	800m
landing speed	20m/s
landing altitude ASL	500m
limit load positive	5g at cruise speed and altitude
limit load negative	-2g at cruise speed and altitude
Safety requirements	
safety factor (SF)	1.5
knockdown factor (KDF)	(B-basis) 90ºC/W/BVID
stiffness	average value
strength	1/SF*KDF*material allowables
buckling	SF*(B-basis KDF)*critical load
1g shape requirement	
twist	linear variation root to tip: 0° to -2°
twist tolerance	+/- 0.05°
tip deflection	no requirement

3.2 Optimization specifications

The objective of the design optimization is to minimize the structural mass. In order to enlarge the design space while considering ease of manufacturability, the wing is split into 12 × 1 spanwise and chord-wise design regions as shown in Figure 4. Each design region corresponds to an area of the wing having the same laminate, or effectively the same stiffness. The stacking sequence in the upper and lower skins, front and rear spars are optimized for, while the laminates in the ribs are pre-defined. Additionally, the leading edge, trailing edge and flaps are not a part of the optimization exercise.
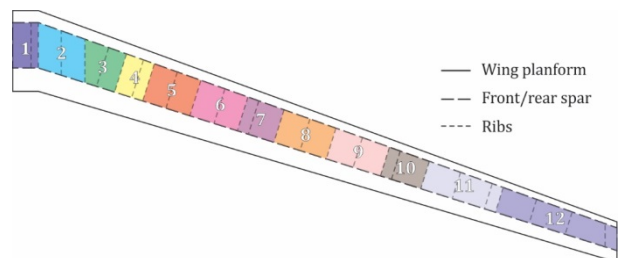

Figure 4: Wing design region distribution

In order to compare the performance of the wings, a constraint on the 1g cruise shape was placed in the optimization. This ensured that benefits attained through aeroelastic tailoring did not come at the expense of aerodynamic performance. A linear twist distribution with 0° at the root and -2° at the tip, at 1g cruise was included in the optimization. The optimization objectives, responses and load-cases are summarized in Table 2.

Table 2: Aereoelastic tailoring optimization - summary

Optimization responses	
objective	mass – minimization
outputs	blended stacking sequence jig-twist
physical constraints	laminate strength buckling tip-twist (at 1g cruise) static divergence aileron effectiveness, $\eta > 15\%$
laminate constraints	10% rule [] symmetry ply contiguity (max. 4) $\pm 45°$ outer plies max. disorientation of 45° balance (for reference wing)
sizing loadcases	+5g at 45m/S (TAS) -2g at 45m/s (TAS)

4. OPTIMIZATION RESULTS

In order to provide a comparable basis for the aeroelastic tailoring demonstration, two wings are designed using the aeroelastic tailoring framework described in the previous sections. The first reference wing is designed with balanced-symmetric type of laminates, while the tailored wing is restricted only to symmetric laminates. The tailored wing thus has a larger design-space and should be able to better tap the bending-torsion capabilities of anisotropic composites to design more efficient wings.

The optimization results obtained from the first optimization step using PROTEUS have been detailed in [5]. Along with the optimal stiffness design of the wing, this first step also provides with the optimal jig-twist. This jig-twist is then utilized directly in the stacking sequence optimization. The results from the second stacking sequence optimization step are the focus of the section here.
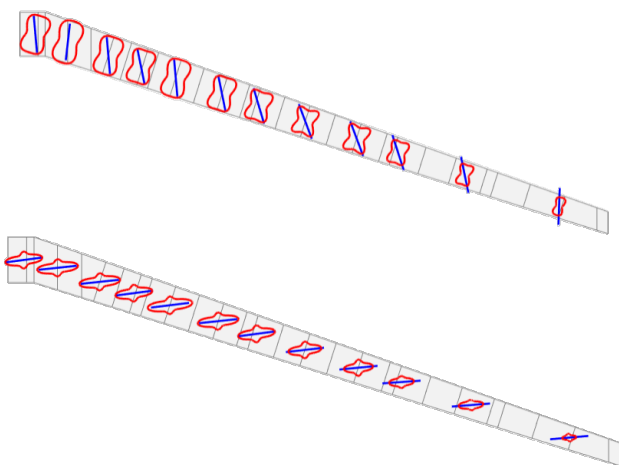
Figure 5: Polar distribution of in-plane stiffness term A_{11} in the reference design (top) and tailored design (bottom), for the upper skin
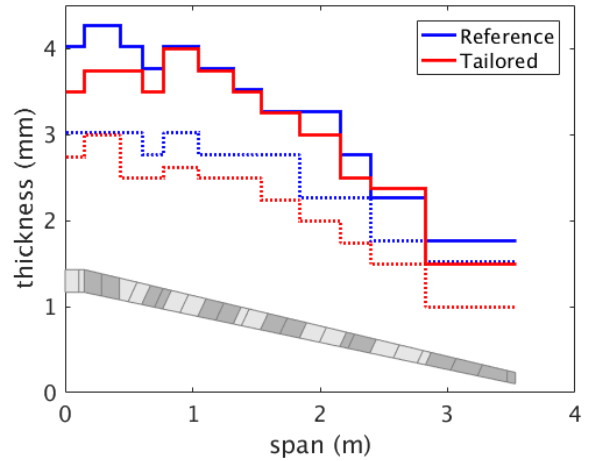
Figure 6: Thickness distribution in the reference and tailored wing along the span, in the upper skin

The wing-box mass is chosen is as the optimization objective to be minimized. The optimal mass of the two wings shown in Table 3 highlights two important points. Firstly, the tailored wing's final stacking sequence design corresponds to a mass 6.30kg per wing half, in comparison with 6.88kg for the reference wing. This weight saving of close to 8% arises purely out of the added design space on account of the unbalanced laminates, which then leads to a better use of composite tailoring benefits. Secondly, it is seen that stiffness-optimal designs obtained from the first optimization step in both the reference and tailored wings are between 12-17% heavier than their stacking sequence counterparts. This increase in weight can be expected since the stacking sequence design is constrained by the discrete steps of ply angles and thickness. Additionally, the stacking sequence design includes the constraint of laminate blending and the additional laminate guidelines. The increase in weight in the stacking sequence design can be attributed to these reasons, which are not accounted for in the stiffness-optimization step.

Table 3: Wing-box mass (one half) of the reference and tailored wing design (the design from the PROTEUS optimization step is denoted as Stiffness-opt., and the design from the stacking sequence optimization step is denoted as Stacking-seq.)

	Mass (kg)	Root bending moment (Nm)		
		1g	5g	-2g
Stiffness-opt. (reference)	5.884	304	1662	726
Stiffness-opt. (tailored)	5.652 (0.96)	305 (1.00)	1555 (0.94)	647 (0.89)
Stacking seq. (reference)	6.878	310.95	1697.65	-729.61
Stacking seq. (tailored)	6.307 (0.92)	314.17 (1.01)	1651.86 (0.97)	-689.01 (0.94)

The comparatively better performance of the tailored wing is a direct result of the added design space offered by unbalanced laminates. This is evident in Figure 5, which show the polar distribution of the A_{11} term of the in-plane stiffness matrix in the upper skin. The highly anisotropic stiffness distribution in the tailored wing results in the classic bend-twist composite coupling that produces a nose-down twist upon upward bending.

Consequently, a pull-up manoeuvre for instance produces a nose-down twist, which in turn results in an inboard-shifting of loads and finally, in an alleviated root bending moment as listed in Table 3. The reduced loads result in lesser thickness requirements as shown in Figure 6, leading to the savings in weight.

This in-board shift of the lift in the tailored design is visible in Figure 7, which shows the span-wise lift distribution in the wing for different manoeuvre loads. The structural wing twist in the wings is shown in Figure 8. A negative structural twist implies a nose-down twist, which is beneficial in a pull-up manoeuvre to alleviate loads. This negative structural twist in the case of the 5g manoeuvre load is significantly larger in the tailored wing, which in turn helps in shifting the loads in-board.
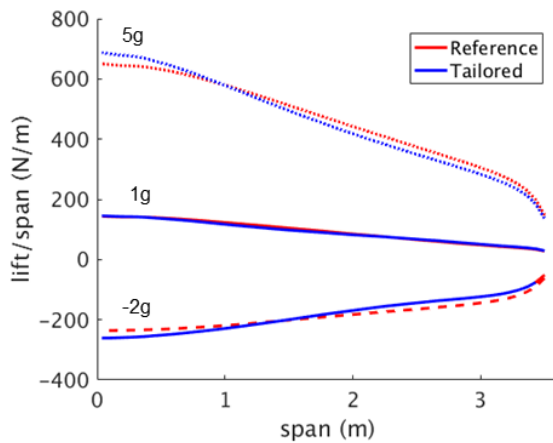

Figure 7: Span-wise lift distribution in the reference and tailored wings, for different manoeuvre loads
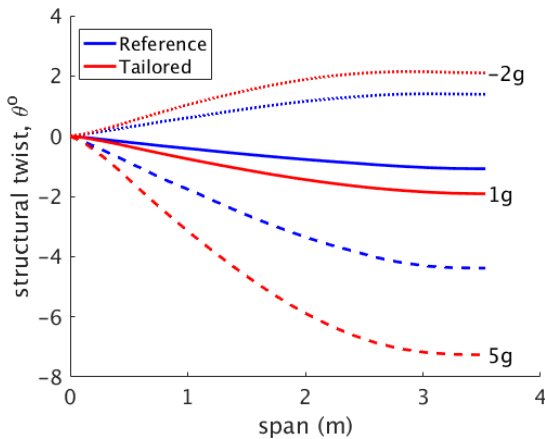

Figure 8: Span-wise structural twist distribution in the reference and tailored wings for different manoeuvre loads

5. MANUFACTURING OF WINGS

The reference and the tailored wing are built using carbon fibre reinforced plastic (CFRP) material at FACC (Austria), a partner participating in the project. All of the large structural components such as wing skins, spars, leading edge connection strip and ribs are built using standard aerospace grade carbon fibre unidirectional prepreg material designated AS4-8552. The layup of the CFRP material comprising the wing skins and the spars is based on the optimisation results presented earlier.

To be able to manufacture the wings, a set of curing and assembly tools are developed as shown in Figure 9a. Female CFRP curing tools are selected for the wing skins to avoid interference effects due to mismatch in thermal expansion between the carbon fibre part and the curing tool. In addition, CFRP curing tools allow for the adjustment of their geometry, enabling the use of the same curing tool for both reference as well as the tailored wing, which leads to significant cost reduction of the required curing tools. Conventional aluminium curing tools are used for manufacturing of the spars and the leading-edge connection strip, since these components are not so sensitive to the thermal expansion mismatch, due to their small surface area.
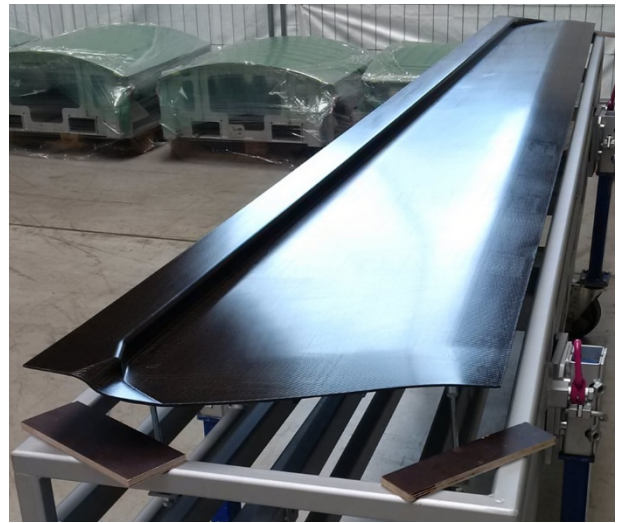
a.) CFRP mould for the wing skin

b.) Metal moulds for the front and rear spars

Figure 9: Curing tools for manufacturing of the reference and the tailored wing

Sequential adhesive bonding is then used to join individual components in larger sub-assemblies and into the final assembly. Smaller components such as flap actuation brackets and flap close-out ribs are 3D-printed.

Additional sub-systems including fibre Bragg grating (FBG) sensors, on-board accelerometers, electrical equipment, inertial measurement units (IMUs), servo actuators, health monitors for servo actuators and the necessary cabling are integrated into the wing.
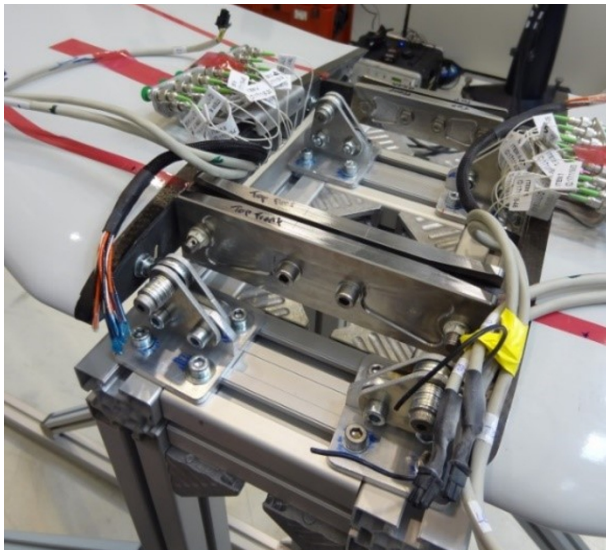
6. STATIC TEST AND MODEL UPDATE

Generally speaking, aeroelastic problems deal with the interaction between structural, aerodynamic and inertial loads. In addition to modelling assumptions, the modelled aeroelastic response can differ from the measured response due to possible discrepancies between the numeric model and the built physical model. The main discrepancies originate from the differences in mass and stiffness distribution and from the geometric imperfection in the aerodynamic shape of the test specimen.
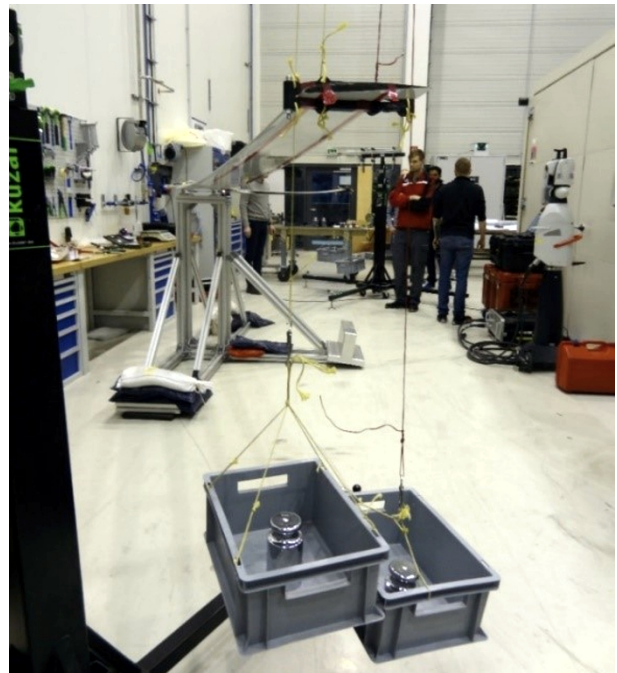
6.1 Setup

The main objective of the static test is the assessment of the stiffness properties of the manufactured reference wing and validation of the pertinent structural models developed and utilized in the design process. A pair of reference wings is mounted in a dedicated test-stand as shown in Figure 10a. In order to achieve representative boundary conditions at the root of the wing, both port and starboard half of the wing are mounted in the test-stand and connected in the middle. Prescribed loads are then applied to both halves in a symmetric fashion as illustrated in Figure 10b.

Discrete loads are applied by hanging weights at predetermined locations along the span of the wing as depicted in Figure 11. To avoid accidentally damaging the wing structure during the test, a set of maximum shear and torque loads are determined for each span-wise location and load direction. Altogether 18 load-cases are tested for the different load-positions and load magnitudes. In addition, load clamps fitted to the wing shape are used to spread the load gradually into the wing structure to avoid causing any structural damage due to local stress concentrations.

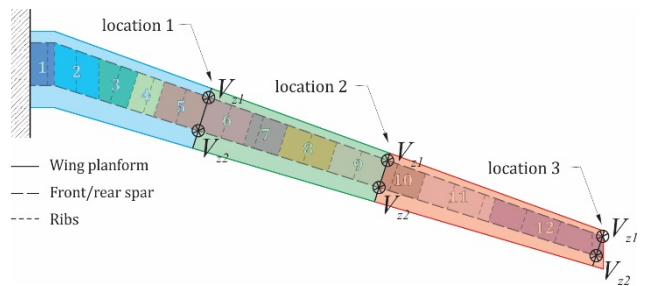b.) Static load application

Figure 10: Static test setup

Figure 11: Load application points

6.2 Results

Measured deflections in terms of bending displacement and torsional rotation are compared to numerical predictions in this section. Numerical predictions are obtained using the aeroelastic tools developed by TUD and DLR. The comparison results are also used for updating the stiffness properties of the two numerical models and is briefly described below.

6.2.1 PROTEUS beam-model

Initial comparison between the numerical model and the static test for a selected load case is shown in Figures 13 and 14. The comparison is shown in terms of bending deflection and torsional rotation along the span. The dotted line represents the measurements and the dashed line represents the initial numerical results. An average difference of about 50% is observed which is attributed to the difference in the support boundary condition at the root of the wing. In the numerical model the wing support is modelled as an ideal rigid clamp, while the boundary condition in the experiment and the flying aircraft is essentially elastic, which leads to considerably larger deflections measured during the experiment.
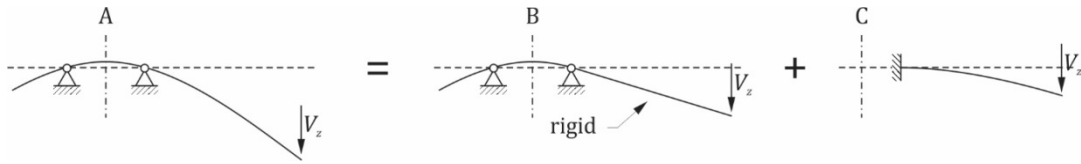

a.) Wing clamped to the test stand

Figure 12: Wing support and boundary condition

Assuming a linear structural response, the measured bending deflection of the wing (A as shown in Figure 12) can be considered as a sum of rigid body rotation due to support flexibility (B) and elastic deflection due to wing flexibility (C). By accounting for the rigid body rotation component of the measured experimental deflection, effective support stiffness for bending and torsion can be estimated. Adding this root-flexibility into the simulation models in the form of an attachment-stiffness update, a very good correlation is obtained between the simulation models and the experimental results, as shown for one load case in Figures 13 and 14.
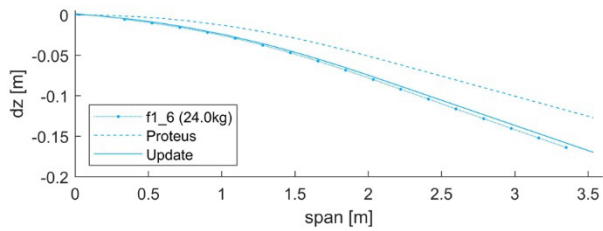

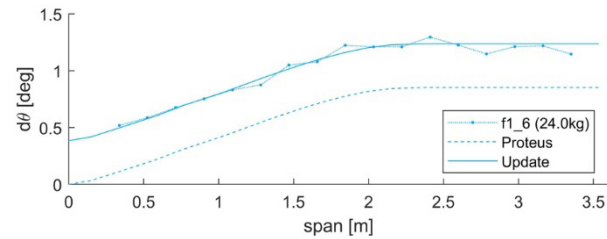Figure 13: Initial and updated PROTEUS model vs. experimental results – span-wise displacement

Figure 14: Initial and updated PROTEUS model vs. experimental results – span-wise twist

6.2.2   NASTRAN shell-model

A comparison between the initial NASTRAN FE model used in the stacking sequence optimization and the experimental results for a selected load case is shown in Figure 15. The FE model corresponds to the optimized design obtained in the second optimisation step as described earlier. It is seen that a maximum deviation of close to ~20% is observed in the tip-displacement between the FE model and the physical structure. This difference can be attributed to several reasons – modelling assumptions and simplifications, manufacturing deviations, material scatter etc. It is to be noted that FE model contains a reasonable representation of the actual boundary conditions of the wing.

In order to update the FE model using information from the performed static tests, a model-updating is performed. For this step, an approach using 'tuning beams' is used. Several beams are added, attached to the wing model and the stiffness of these beams are 'tuned' such that the effective stiffness of the wing plus beam matches the experimental results. With this relatively simple model-updating approach, the stiffness of the FE models is updated for one load case and is shown in Figure 17 to match the experimental results very well in other load cases as well.
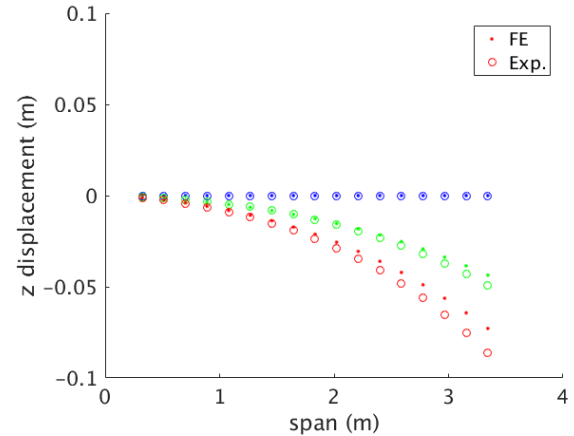

Figure 15: Initial FE model vs. experimental results – span-wise displacement (different colours representing the different load-magnitudes)
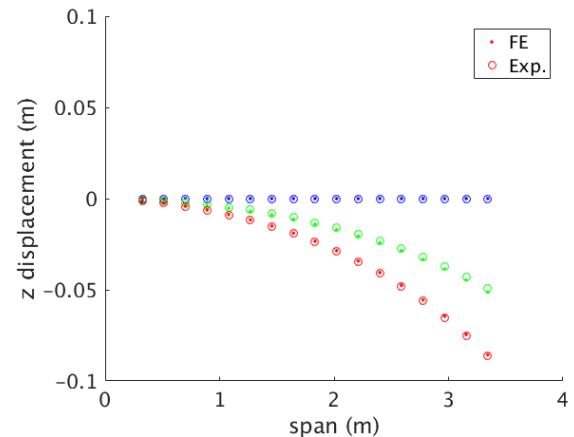

Figure 16: Updated FE model vs. experimental results – span-wise displacement (different colours representing the different load-magnitudes)

In the tuning beam approach used here, only the bending stiffness – related parameters of the tuning beams are used for the model-update. The torsional deformation from the experiments however shows some scatter in the test-points as shown in Figure 17. This can be explained given the very small twist expected in the first place and the limitations of the test-setup and the displacement measurement capabilities. Fitting the measured data for use in a model-update is hence difficult. The measured twist values however are reasonably close to the FE models already; hence, no

7

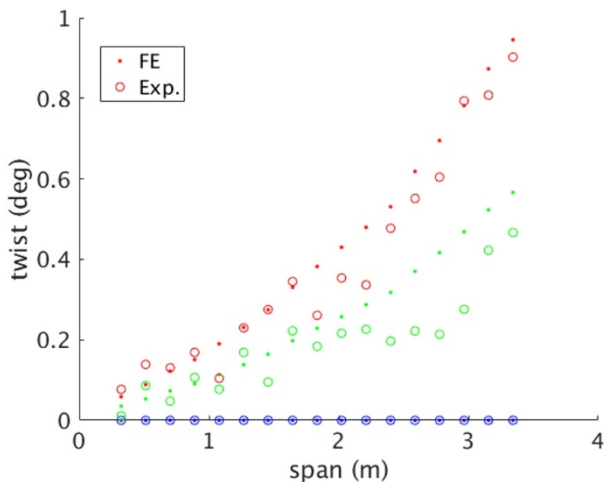model-update is performed using the experimentally-measured twist deformations.

Figure 17: FE model vs. experimental results – span-wise twist (different colours representing the different load-magnitudes)

7. AIRWORTHINESS TEST

In addition to the static tests, an airworthiness test is performed on the reference wing in order to confirm that the wing can sustain the limit design loads, namely 5g and -2g for which it is designed. An impression from the test-stand and the deformed wing is shown in Figure 18. The wing is loaded with a 5g and -2g equivalent load by hanging sand bags at six span-wise locations on either side of the wings. In the case of the -2g loads, the wing flipped over before applying the loads.

The equivalent loads are derived by matching the deflected shape under the limit loads. This way the loads to be applied, the resulting shear force and the bending moment along the span are recovered, as shown in Figure 19 as an example for 1g loads. One can observe that the equivalent shear force changes in discrete steps due to the fact that the forces are applied at discrete locations along the span of the wing. Nevertheless, the equivalent bending moment follows the bending moment in flight very faithfully.

The airworthiness test of the reference wing shows, that the wing can sustain the limit loads without any detectable structural damage and is therefore deemed safe to operate.
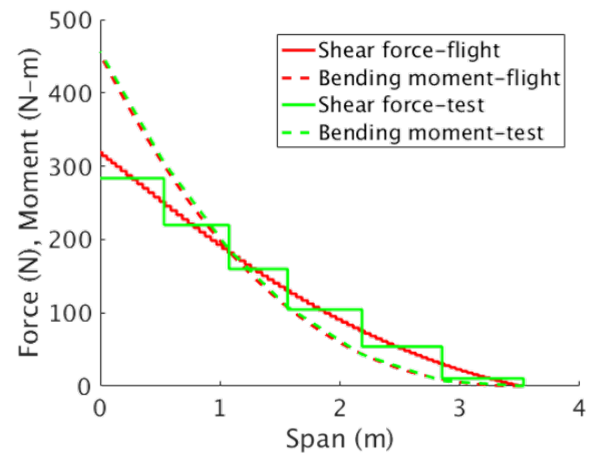

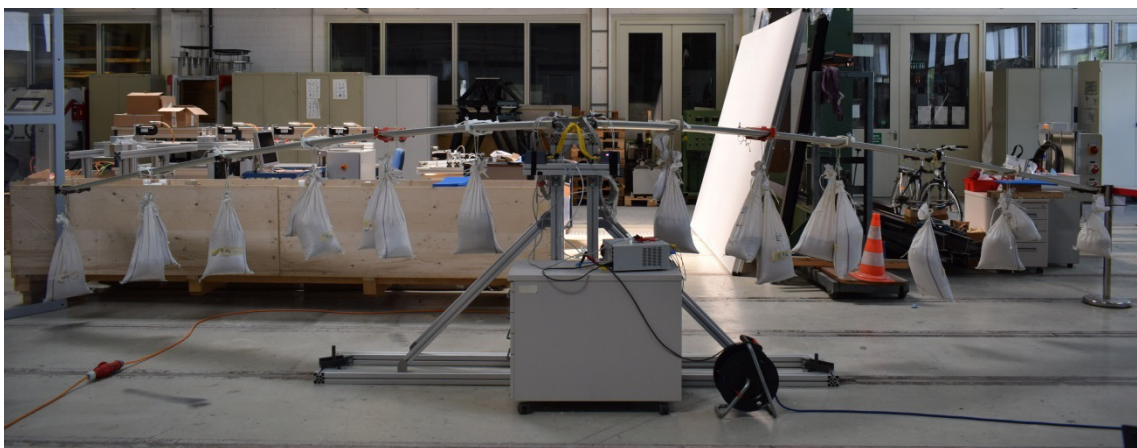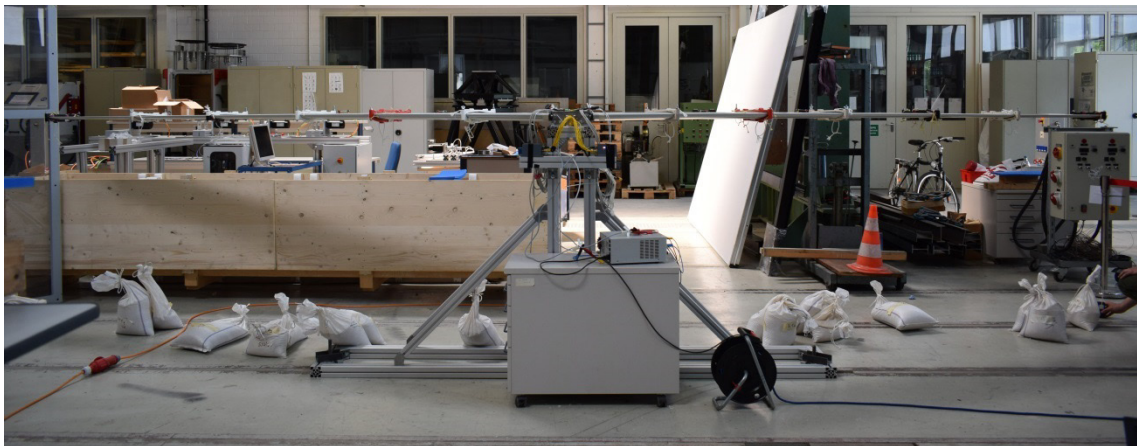Figure 19: Derivation of the equivalent 1g limit loads

Figure 18: Airworthiness test – stand-stand (above) and loaded wings (below)

8. GROUND VIBRATION TESTS (GVT)

With the simulation models of the wings updated from a stiffness-perspective using the static test results, GVTs will be performed next in which the dynamic behaviour of the wings will be characterized.

In the case of the GVTs, the full UAV will be instrumented with accelerometers, suspended on elastic strings and excited with an impulse hammer. From the time-response of the accelerometers, a modal analysis will be performed to obtain the eigen frequencies, mode shapes and damping corresponding to each of the modes. The results will then be used to update the FE models of the full UAV aircraft, which are critical for the final controller designs in the next phase.

9. FLIGHT TEST

The planned flight tests with the FLEXOP UAV involve a test-leg with a horse-race pattern as shown in Figure 20. The manoeuver-loads that will be tested for the aeroelastic tailoring demonstration will be introduced during coordinated turns.

The FBGs on-board will record the in-flight strains. The measured strains along with dedicated shape sensors instrumented in the FBGs will be used to calculate deformations (displacement and twist), sectional loads and the wing root bending moment. The difference in the root bending moments, the sectional loads and the bending-torsion coupling induced twist during introduced manoeuvres, between the reference and tailored wing designs are crucial measures in evaluating the aeroelastic tailoring capability of the applied framework. Additionally, an update of the aeroelastic models will also be based on these measurements.

During the flight tests, acceleration data from the on-board accelerometers will also be recorded, which together with the recorded flight-parameters, will be used to perform in-flight system identification.
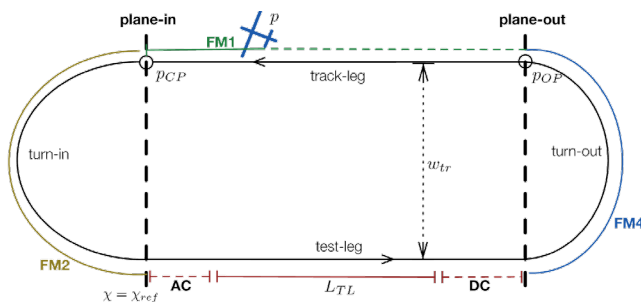

Figure 20: Test-leg for the FLEXOP UAV

10. CONCLUSION AND OUTLOOK

A joint DLR – TUD aeroelastic tailoring framework is applied in the design of two pairs of wings. The goal of this endeavour is to demonstrate the aeroelastic tailoring framework on an actual flying test-bench, while going through an entire cycle of design, optimization, manufacturing and testing of an aircraft – the FLEXOP UAV in this case.

In order to enable a fair demonstration of aeroelastic tailoring, the first reference pair of wings is designed using conventional balanced-symmetric laminates, while the second tailored paired of wings is designed using symmetric laminates, thus allowing for better use of the beneficial bending-torsion coupling of composite laminates. The wing-box comprising of upper and lower skins, front and rear spars, is optimized and the optimization results show a weight saving potential of ~8% when comparing the tailored with the reference design.

The optimized baseline wing has been manufactured at the present stage. A static test campaign is performed to characterize the stiffness behaviour of the physical wing. The measured experimental data has been used to verify and update the simulation models from a stiffness perspective. Additionally, an airworthiness test is successfully performed to test the wing under the designed limit loads.

The next step is to perform GVTs on the entire UAV configuration and to update its dynamic behaviour. The results from this task would flow into the controller design groups, in updating the models for the control synthesis. A dedicated flight test campaign will also be performed in order to validate the aeroelastic tailoring framework and the aeroelastic models that have been developed during the course of this work.

Finally, the tools developed and the lessons learnt during the course of the FLEXOP project will be used in scaling-up this design exercise to a practical, commercial-scale aircraft wing.

11. ACKNOWLEDGEMENT

12. BIBLIOGRAPHY

[1] FLEXOP Consortium, "The FLEXOP Project," 2013. .

[2] P. Stahl, F.-M. Sendner, A. Hermanutz, C. Rößler, and M. Hornung, "Mission and Aircraft Design of FLEXOP Unmanned Flying Demonstrator to Test Flutter Suppression within Visual Line of Sight," presented at the 17th AIAA Aviation Technology, Integration, and Operations Conference, Denver, Colorado, 2017.

[3] F.-M. Sendner, P. Stahl, C. Rössler, and M. Hornung, "Design of an Electric Actuated Airbrake for Dynamic Airspeed Control of an Unmanned Aeroelastic Research UAV," 2018.

[4] M. Wuestenhagen, T. Kier, Y. M. Meddaikar, M. Pusch, D. Ossmann, and A. Hermanutz, "Aeroservoelastic Modeling and Analysis of a Highly Flexible Flutter Demonstrator," 2018.

[5] J. Sodja, N. Werter, and R. De Breuker, "Design of a flying demonstrator wing for manoeuvre load alleviation with cruise shape constraint," 2018.

[6] V. Rozov, A. Hermanutz, C. Breitsamter, and M. Hornung, "AEROELASTIC ANALYSIS OF A FLUTTER DEMONSTRATOR WITH A VERY FLEXIBLE HIGH-ASPECT-RATIO SWEPT WING," presented at the

IFASD 2017 (International Forum on Aeroelasticity and Structural Dynamics), Como, Italy, p. 13.

[7]   M. H. Shirk, T. J. Hertz, and T. A. Weisshaar, "Aeroelastic tailoring - Theory, practice, and promise," *Journal of Aircraft*, vol. 23, no. 1, pp. 6–18, Jan. 1986.

[8]   F. E. Eastep, V. A. Tischler, V. B. Venkayya, and N. S. Khot, "Aeroelastic Tailoring of Composite Structures," *Journal of Aircraft*, vol. 36, no. 6, pp. 1041–1047, Nov. 1999.

[9]   J. K. S. Dillinger, M. M. Abdalla, T. Klimmek, and Z. Gurdal, "Static Aeroelastic Stiffness Optimization and Investigation of Forward Swept Composite Wings," presented at the 10th World Congress on Structural and Multidisciplinary Optimization, Orlando, Florida, USA, 2013, p. 10.

[10]   S. J. Guo, J. R. Bannerjee, and C. W. Cheung, "The effect of laminate lay-up on the flutter speed of composite wings," *Proceedings of the Institution of Mechanical Engineers, Part G: Journal of Aerospace Engineering*, vol. 217, no. 3, pp. 115–122, Mar. 2003.

[11]   Abdalla, Mostafa M., De Breuker, Roeland, and Gürdal, Zafer, "Aeroelastic tailoring of variable-stiffness slender wings for minimum compliance," presented at the IFASD 2017 (International Forum on Aeroelasticity and Structural Dynamics), Stockholm, Sweden, p. 10.

[12]   J. K. S. Dillinger, T. Klimmek, M. M. Abdalla, and Z. Gürdal, "Stiffness Optimization of Composite Wings with Aeroelastic Constraints," *Journal of Aircraft*, vol. 50, no. 4, pp. 1159–1168, Jul. 2013.

[13]   M. Kameyama and H. Fukunaga, "Optimum design of composite plate wings for aeroelastic characteristics using lamination parameters," *Computers & Structures*, vol. 85, no. 3–4, pp. 213–224, Feb. 2007.

[14]   G. N. Vanderplaats and T. A. Weisshaar, "Optimum design of composite structures," *International Journal for Numerical Methods in Engineering*, vol. 27, no. 2, pp. 437–448, Sep. 1989.

[15]   S. Guo, W. Cheng, and D. Cui, "Aeroelastic Tailoring of Composite Wing Structures by Laminate Layup Optimization," *AIAA Journal*, vol. 44, no. 12, pp. 3146–3150, Dec. 2006.

[16]   Y. M. Meddaikar, J. K. Dillinger, J. Sodja, H. Mai, and R. De Breuker, "Optimization, Manufacturing and Testing of a Composite Wing with Maximized Tip Deflection," 2016.

[17]   Y. M. Meddaikar, J. K. S. Dillinger, M. Ritter, and Y. Govers, "OPTIMIZATION & TESTING OF AEROELASTICALLY-TAILORED FORWARD SWEPT WINGS," presented at the IFASD 2017 (International Forum on Aeroelasticity and Structural Dynamics), Como, Italy, p. 17.

[18]   J. Sodja, N. Werter, J. K. Dillinger, and R. De Breuker, "Dynamic Response of Aeroelastically Tailored Composite Wing: Analysis and Experiment," 2016.

[19]   N. P. M. Werter and R. De Breuker, "A novel dynamic aeroelastic framework for aeroelastic tailoring and structural optimisation," *Composite Structures*, vol. 158, pp. 369–386, Dec. 2016.

[20]   E. Ferede and M. Abdalla, "Cross-sectional modelling of thin-walled composite beams," 2014.

[21]   R. De Breuker, M. M. Abdalla, and Z. Gürdal, "A Generic Morphing Wing Analysis and Design Framework," *Journal of Intelligent Material Systems and Structures*, vol. 22, no. 10, pp. 1025–1039, Jul. 2011.

[22]   N. P. M. Werter, R. De Breuker, and M. M. Abdalla, "Continuous-Time State-Space Unsteady Aerodynamic Modeling for Efficient Loads Analysis," *AIAA Journal*, vol. 56, no. 3, pp. 905–916, Mar. 2018.

[23]   M. Miki and Y. Sugiyama, "Optimum design of laminated composite plates using lamination parameters," 1991.

[24]   H. Fukunaga and G. N. Vanderplaats, "Stiffness Optimization of Orthotropic Laminated Composites Using Lamination Parameters," *AIAA Journal*, vol. 29, no. 4, pp. 641–646, Apr. 1991.

[25]   H. Fukunaga and H. Sekine, "Stiffness design method of symmetric laminates using lamination parameters," *AIAA Journal*, vol. 30, no. 11, pp. 2791–2793, Nov. 1992.

[26]   Y. M. Meddaikar, F.-X. Irisarri, and M. M. Abdalla, "Laminate optimization of blended composite structures using a modified Shepard's method and stacking sequence tables," *Structural and Multidisciplinary Optimization*, vol. 55, no. 2, pp. 535–546, Feb. 2017.

[27]   F.-X. Irisarri, A. Lasseigne, F.-H. Leroy, and R. Le Riche, "Optimal design of laminated composite structures with ply drops using stacking sequence tables," *Composite Structures*, vol. 107, pp. 559–569, Jan. 2014.

[28]   J. van Campen, O. Seresta, M. Abdalla, and Z. Gürdal, "General Blending Definitions for Stacking Sequence Design of Composite Laminate Structures," 2008.

[29]   T. Klimmek, "Parameterization of Topology and Geometry for the Multidisciplinary Optimization of Wing Structures," presented at the CEAS 2009 European Air and Space Conference, 2009, p. 9.